Daily High-Resolution Temperature and Precipitation Fields for the Contiguous United States from 1951 to Present

IMKE DURRE,[a] ANTHONY ARGUEZ,[a] CARL J. SCHRECK III,[b] MICHAEL F. SQUIRES,[c] AND RUSSELL S. VOSE[a]

[a] *NOAA/National Centers for Environmental Information, Asheville, North Carolina*
[b] *Cooperative Institute for Satellite Earth System Studies, North Carolina State University, Asheville, North Carolina*
[c] *Saint Louis, Missouri*

(Manuscript received 28 February 2022, in final form 5 July 2022)

ABSTRACT: In this paper, a new set of daily gridded fields and area averages of temperature and precipitation is introduced that covers the contiguous United States (CONUS) from 1951 to present. With daily updates and a grid resolution of approximately 0.0417° (nominally 5 km), the product, named nClimGrid-Daily, is designed to be used particularly in climate monitoring and other applications that rely on placing event-specific meteorological patterns into a long-term historical context. The gridded fields were generated by interpolating morning and midnight observations from the Global Historical Climatology Network–Daily dataset using thin-plate smoothing splines. Additional processing steps limit the adverse effects of spatial and temporal variations in station density, observation time, and other factors on the quality and homogeneity of the fields. The resulting gridded data provide smoothed representations of the point observations, although the accuracy of estimates for individual grid points and days can be sensitive to local spatial variability and the ability of the available observations and interpolation technique to capture that variability. The nClimGrid-Daily dataset is therefore recommended for applications that require the aggregation of estimates in space and/or time, such as climate monitoring analyses at regional to national scales.

SIGNIFICANCE STATEMENT: Many applications that use historical weather observations require data on a high-resolution grid that are updated daily. Here, a new dataset of daily temperature and precipitation for 1951–present is introduced that was created by interpolating irregularly spaced observations to a regular grid with a spacing of 0.0417° across the contiguous United States. Compared to other such datasets, this product is particularly suitable for monitoring climate and drought on a daily basis because it was processed so as to limit artificial variations in space and time that may result from changes in the types and distribution of observations used.

KEYWORDS: North America; Data processing/distribution; Surface observations; Interpolation schemes; Climate services

1. Introduction

Operational climate monitoring activities under the National Oceanic and Atmospheric Administration (NOAA) and the National Integrated Drought Information System (NIDIS) center on the publication of regular reports that summarize recent conditions and long-term trends at various spatial scales across the United States. They rely primarily on monthly gridded fields of temperature and precipitation (hereafter referred to as nClimGrid-Monthly; Vose et al. 2014) and various indicators derived from them, such as the Palmer drought severity index (PDSI; Palmer 1965). Compared to irregularly spaced station observations, which contain missing reports and are preferentially located at lower elevations, gridded fields are temporally and spatially complete. Although each grid-point value is, by nature, an estimate of the actual conditions within each grid box during a particular time interval, a gridded field tends to provide more representative spatial patterns than point observations. In addition, data on a regular grid can be easily aggregated over various geographic entities, such as climate regions or river basins, and yield more accurate regional averages than station observations (Vose et al. 2014).

Increasingly, the users of climate and drought monitoring reports, including water resource managers, farmers, and other decision-makers, are in need of more timely climate information than can be provided on a monthly time scale. For example, accurate weekly drought monitoring requires calculations of indicators for the most recent 90-day periods at the end of each week. In addition, the heat waves, cold-air outbreaks, and flooding events of recent years have heightened interest in understanding the degree of unusualness of such submonthly events among planners, the media, and the general public.

The fulfillment of these needs necessitates a set of daily, rather than monthly, gridded fields of temperature and precipitation covering at least the contiguous United States (CONUS) that are updated in near–real time. While many station observations are already available with a latency of 1–3 days, regularly updated grids of daily temperature and precipitation with a spatial resolution of no more than a few kilometers are needed in order to allow for the generation of geographically representative maps and area averages of meteorological events as they emerge. To facilitate the comparison of current events with past conditions, a practice that is central to climate monitoring activities, the gridded fields must span as much of the historical record as is feasible given that the spatial coverage of the observations becomes increasingly limited going backward in time from the late 1900s. Further, the effects of temporal

Corresponding author: Imke Durre, imke.durre@noaa.gov

DOI: 10.1175/JTECH-D-22-0024.1

inhomogeneities, such as those resulting from changes in the measurement or spatial distribution of the underlying data, need to be minimized to reduce, if not eliminate, the chance that nonclimatic signals mask the climatic long-term trend and variability.

To address these requirements, a set of gridded fields and area averages of daily maximum temperature (Tmax), minimum temperature (Tmin), and precipitation (Prcp) was developed that covers the CONUS (Durre et al. 2022). This new product, called nClimGrid-Daily, is available from NCEI beginning with 1 January 1951 and is kept up to date to within at least 3 days of the current date. The gridded fields are generated by applying thin-plate smoothing splines (TPSS) to quality-controlled observations from the Global Historical Climatology Network–Daily (GHCNd) dataset (Menne et al. 2012a,b). Following the interpolation, additional processing steps ensure both the internal consistency of the interpolated fields and their consistency with nClimGrid-Monthly (Vose et al. 2014). From the daily gridded values, area averages for various types of regions ranging in size from census tracts to the entire CONUS are also calculated.

The TPSS method was chosen for three primary reasons. First, compared to other interpolation approaches, this method is particularly suitable for the wide range of topographical and climatic features of the CONUS as it provides a natural framework for incorporating predictor variables that represent terrain complexity and coastal proximity, factors that have been shown to significantly reduce interpolation errors (Hutchinson 1998b; Jarvis and Stuart 2001a). Second, the TPSS method has been found to be suitable for the interpolation of daily temperature and Prcp at various spatial scales (Haylock et al. 2008; Hutchinson et al. 2009; Herrera et al. 2016). Third, for nClimGrid-Daily in particular, an additional advantage of using TPSS is that this method was also used as part of the creation of its monthly sister dataset, nClimGrid-Monthly (Vose et al. 2014).

While a number of datasets of daily gridded temperature and Prcp fields exist, none of them satisfies all of the requirements of CONUS-wide regional to national climate monitoring applications. For example, the gridded data in the Applied Climate Information System (ACIS; DeGaetano and Belcher 2007) were, like nClimGrid-Daily, developed to support real-time climate monitoring, but were originally designed only for the northeastern United States. The collection of daily fields produced with the Parameterized-Elevation Regressions on Independent Slopes Model (PRISM; Diluzio et al. 2008; Daly et al. 2021) is available free of charge at a high resolution of 4 km within 24 h of the end of each day and reflects the influence of complex terrain features. However, PRISM data are not adjusted for historical changes in measurement practices and do not start until 1981, missing the notable droughts of the 1950s. Daymet (Thornton et al. 1997, 2021) also reflects the effects of terrain and is available at a 1-km resolution, but is only updated monthly. The dataset by Livneh et al. (2015) covers Mexico and Canada in addition to the CONUS and accounts for transboundary discontinuities at the country borders, while Newman et al.'s (2015) Gridded Meteorological Ensemble Tool includes uncertainty estimates, yet neither product is updated routinely. The global-scale datasets described by Huffman et al. (2001), Caesar et al. (2006), Chen et al. (2008), and Contractor et al. (2020) each include either temperature or Prcp, but not both, and are available only at a lower spatial resolution.

This paper is dedicated to describing the methodology for generating nClimGrid-Daily and illustrating the utility and limitations of this new data product. The selection of input data, the interpolation approach, and additional processing steps are described in sections 2–5. Section 6 contains validation results in the form of both cross-validation statistics and illustrative examples of the gridded fields on specific days. In section 7, the utility of nClimGrid-Daily for two climate monitoring applications is assessed. The paper concludes with information on accessing and using nClimGrid-Daily.

2. Preparation of input data

As input to nClimGrid-Daily, reports of Tmax, Tmin, and Prcp were taken from the GHCNd dataset. Containing historical and near-real-time high-quality daily observations from around the world, GHCNd is the most comprehensive source of quality-controlled daily surface observations for the CONUS. GHCNd's CONUS records date back to 1832 and originate from multiple station networks (Menne et al. 2012a,b). Changes in station coverage over time are known to cause temporal variations in the accuracy of associated gridpoint estimates (Chen et al. 2008; Ensor and Robeson 2008; Hofstra et al. 2009; Gervais et al. 2014; Herrera et al. 2019), while spatially and temporally varying observation times can increase interpolation errors and temporal inhomogeneities (DeGaetano 1999; Janis 2002; Daly et al. 2021; Thornton et al. 2021). To limit both of these effects, the available data were subset according to station network and observation time as described below.

a. *Station selection*

To avoid the considerably lower station density of the first half of the twentieth century compared to the second half, the year 1951 was chosen as the first year of analysis. Observations from four prominent networks were used as input to the interpolation algorithm: the Cooperative Observer Program (COOP) and Automated Surface Observing System (ASOS) networks of the National Weather Service (NWS), the Snowpack Telemetry (SNOTEL) network of the U.S. Department of Agriculture's Natural Resources Conservation Service, and the Remote Automatic Weather Stations (RAWS) operated jointly by several wildland management agencies. For RAWS stations, only temperature observations were used because precipitation measurements in this network are typically taken with unheated rain gauges and are therefore unreliable, if not unavailable, under freezing conditions (Zachariassen et al. 2003; Myrick and Horel 2008). Records from the Community Collaborative Rain, Hail and Snow Network (CoCoRAHS) provide excellent national coverage starting around 2010, but were not included in the interpolation because the resulting rapid increase in station density after the year 2000 would have introduced a noticeable temporal inhomogeneity into the gridded dataset.

TABLE 1. Summary of station networks used in nClimGrid-Daily. Acronyms for networks are defined in the text. Acronyms for network operators are defined as follows: BLM = Bureau of Land Management, NRCS = National Resource Conservation Service, and NWS = NOAA National Weather Service. Obs times used refers to the observation times, in local time, that are utilized; observations taken at other times are not considered. Consistent with conventions frequently used in daily NWS reports, the time 2400 refers to local midnight at the end of the reporting day.

Network	Operator	Coverage within CONUS	Period used	Variables used	Obs times used (LT)
COOP	NWS	All states	1951–present	Tmax, Tmin, Prcp	0500–0900, 2400
ASOS	NWS	All states	1992–present	Tmax, Tmin, Prcp	2400
SNOTEL	NRCS	Western states at high elevations	1978–present	Tmax, Tmin, Prcp	2400
RAWS	BLM	Fire-prone locations in foothills and on lower parts of mountain slopes	1983–present	Tmax, Tmin	2400

The coverage, periods of record, and observation times of the four networks are detailed in Table 1, while their instrumentation, siting, observing practices, and measurement errors are documented extensively elsewhere (e.g., Guttman and Baker 1996; Serreze et al. 1999; Zachariassen et al. 2003; Daly et al. 2007; Myrick and Horel 2008; Menne and Williams 2009). Among the available observations, only those that passed all of GHCNd's logical, serial, and spatial quality assurance checks (Durre et al. 2010) were considered as input to nClimGrid-Daily.

b. *Observation time*

A significant challenge of interpolating daily observations is that the time of day at which measurements are taken varies among stations on any given day as well as over time. Different reporting times at neighboring stations can result in differences in the Tmax, Tmin, and Prcp values reported for a given date, even when both sites experience identical conditions (Janis 2002). For example, rainfall from a late morning shower would be included in that same day's 1700 and 2400 LT observations, while 0700 LT observers would include it in their reports for the following morning. Thus, mixing reports from stations with different observing times can introduce spurious spatial variability that can contribute to interpolation errors (e.g., Daly et al. 2021; Thornton et al. 2021). In addition, a change in observation time at a particular location, e.g., from afternoon to morning, can introduce a shift in the mean and variability of the reported observations (Karl et al. 1986; DeGaetano 1999).

Tables 1 and 2 document the network-to-network and temporal variations in observation time within the four networks used for nClimGrid-Daily. Table 2 reflects the gradual shift in reporting time from afternoon to morning that has been taking place throughout the COOP network (e.g., Janis 2002). For the period as a whole, morning, especially the time span of 0500–0900 LT, is the most prominent observation time. While the share of temperature observations at this time of day increased from near 30% to near 70% during 1951–2020, more than half of Prcp measurements were taken in the morning throughout the entire period, and their proportion exceeded 70% by 2020. For nClimGrid-Daily, the next most important observation time is local midnight, as it is the standard reporting time for the RAWS and SNOTEL networks as well as for several hundred COOP and ASOS sites.

To reduce the impact of these observation time variations on the final gridded fields, only measurements taken at the observation times of midnight, 0500, 0600, 0700, 0800, and 0900 LT were considered. For the generation of a given day's gridded field, each day's morning observations were combined with the previous day's midnight observations, thereby maximizing the overlap between the two sets of 24-h observing periods ending at those times. For example, to create the gridded fields for 25 April 2019, measurements taken between 0500 and 0900 LT on that day were combined with reports from 2400 LT 24 April 2019. In a final data selection step, which is explained further below, each midnight measurement from an NWS-operated station that was located within 100 km horizontal distance and within 100 m elevation of a morning-observing station was removed to further limit the impact of

TABLE 2. Distribution of observation times among NWS COOP and ASOS stations at the beginning, middle, and end of the analysis period as represented by 1 Jan in the years 1951, 1985, and 2020. Percentages are relative to all NWS observations whose observation time is documented at NCEI. Times are given on a 24-h clock and refer to local time (e.g., 0500 = 5 a.m. local time, 2400 = midnight at the end of the specified date). Observation times for Tmin are identical to those for Tmax. Only observations between 0500 and 0900 and 2400 LT are used as input to the gridding process.

	1 Jan 1951		1 Jan 1985		1 Jan 2020	
	Tmax	Prcp	Tmax	Prcp	Tmax	Prcp
Total No. of observations	3339	5795	4884	7205	3200	3907
Fraction between 0500 and 0900 LT (%)	33.9	58.4	42.4	61.8	68.6	73.9
Fraction between 1500 and 1900 LT (%)	50.0	31.1	44.0	28.0	8.9	7.6
Fraction at 2400 LT (%)	12.7	7.8	10.7	7.3	20.1	16.7
Fraction at other times (%)	3.4	2.7	2.9	2.9	2.4	1.8

mixing observation times when such mixing does not significantly enhance spatial coverage. The resulting set of input data for each day consists primarily of morning observations, with midnight observations from the previous day, especially those from the RAWS and SNOTEL stations in the mountainous West, filling in significant spatial gaps. It therefore represents conditions that prevailed during the 24 h ending sometime during the first 9 h of the day.

These methodological choices were based on a variety of sensitivity tests with various configurations of networks and observation times as well as a visual assessment of the spatial coverage that each of these configurations would yield at various times throughout the period of analysis. In addition, several methods for handling reports with different observation times were tested. All tests assumed that, at a minimum, measurements taken at the predominant morning observation times of 0500–0900 LT would be utilized. The tests yielded three major findings. First, the addition of afternoon observations from the same or previous day yielded larger interpolation errors, consistent with knowledge about the differences in Tmax, Tmin, and Prcp reported at those two times of day (Karl et al. 1986; Janis 2002). Similarly, combining morning observations with the next later midnight observations (2400 LT on the same date) resulted in larger interpolation errors than combining with the next earlier midnight observations (2400 LT on the previous day). The previous day's midnight reports improved the interpolation results compared to morning observations alone when they also filled in gaps in spatial coverage.

A final set of tests analyzed how large the gap in the spatial coverage of morning observations must be in order for the additional midnight observation to add value. When midnight and morning stations are in close proximity to each other, differences between the observed values are more likely to be the result of the difference in observation time than of their geographical separation, particularly for Tmin and Prcp. An initial analysis of the separation distance between all pairs of stations showed that nearby midnight and morning observations were particularly common in the NWS network, whereas SNOTEL and RAWS stations are predominantly more isolated. Within the NWS network, a comparison of the interpolation errors for a range of combinations of distance and elevation difference thresholds between midnight and morning stations showed that the errors remained consistent for thresholds around 100 km horizontal separation and 100 m vertical separation and increased as thresholds were lowered significantly below these values. The use of these thresholds results in the exclusion of 300–400 midnight observers on any given day.

c. *Resulting data coverage*

Figure 1 contains time series of the relative contribution of each constituent network and observation time category (morning or midnight) in the input data after the above data selection steps have been applied. In Fig. 2, maps depict the spatial distribution of observations at the beginning and end of the record analyzed as well as on the day with the largest number of observations. Morning COOP observations dominate throughout

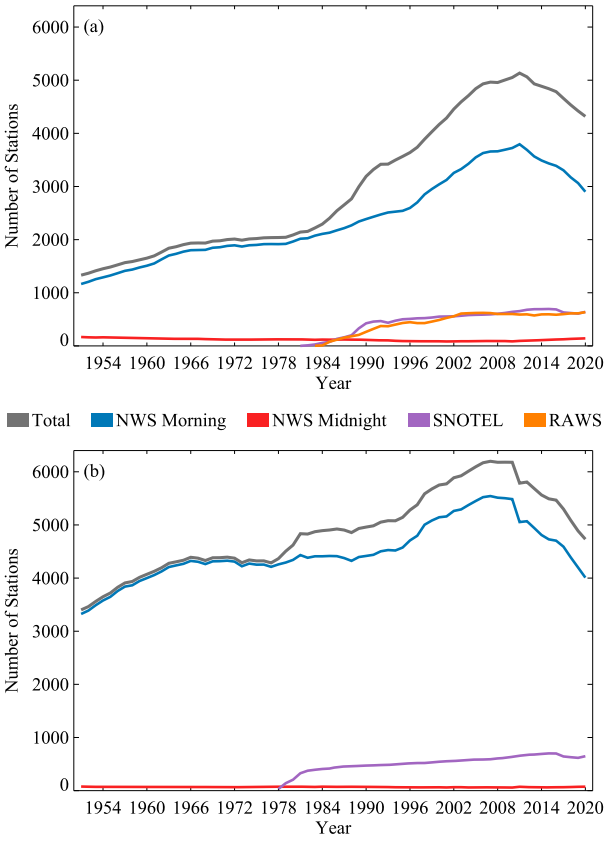

FIG. 1. Average number of stations used in nClimGrid-Daily for each year between 1951 and 2020 for (a) temperature and (b) precipitation. Shown are the total annual station count (gray) and annual numbers of NWS morning (blue), NWS midnight (red), SNOTEL (purple), and RAWS (orange) sites.

the record, and there are consistently more stations for Prcp than for temperature, owing to the greater density of Prcp observers compared to temperature observers in the COOP network (Fig. 1). The total number of observations used increases from around 1300 (3400) for temperature (Prcp) in 1951 to over 5000 (6000) in the late 2000s. This increase is the result of a general rise in the number of morning COOP observations and of the introduction of the SNOTEL and RAWS networks starting in the 1980s. The coverage in 2020 (Figs. 2c,f) is generally similar to 2009 (Figs. 2b,e), although the density of NWS morning sites thins between 2009 and 2020, consistent with the decrease in the overall number of stations during that time (Fig. 1).

Midnight observations augment the spatial coverage of the morning observations. In the western half of CONUS, the coverage is somewhat sparse for both temperature and Prcp in the early 1950s (Figs. 2a,d), but improves significantly over time, especially with the addition of SNOTEL and RAWS sites, most of which are situated in remote locations of the western mountains and foothills (Serreze et al. 1999; Myrick and Horel 2008). In the East, midnight observations from NWS stations are particularly useful for filling in gaps in temperature observations early in the record (Fig. 2a).

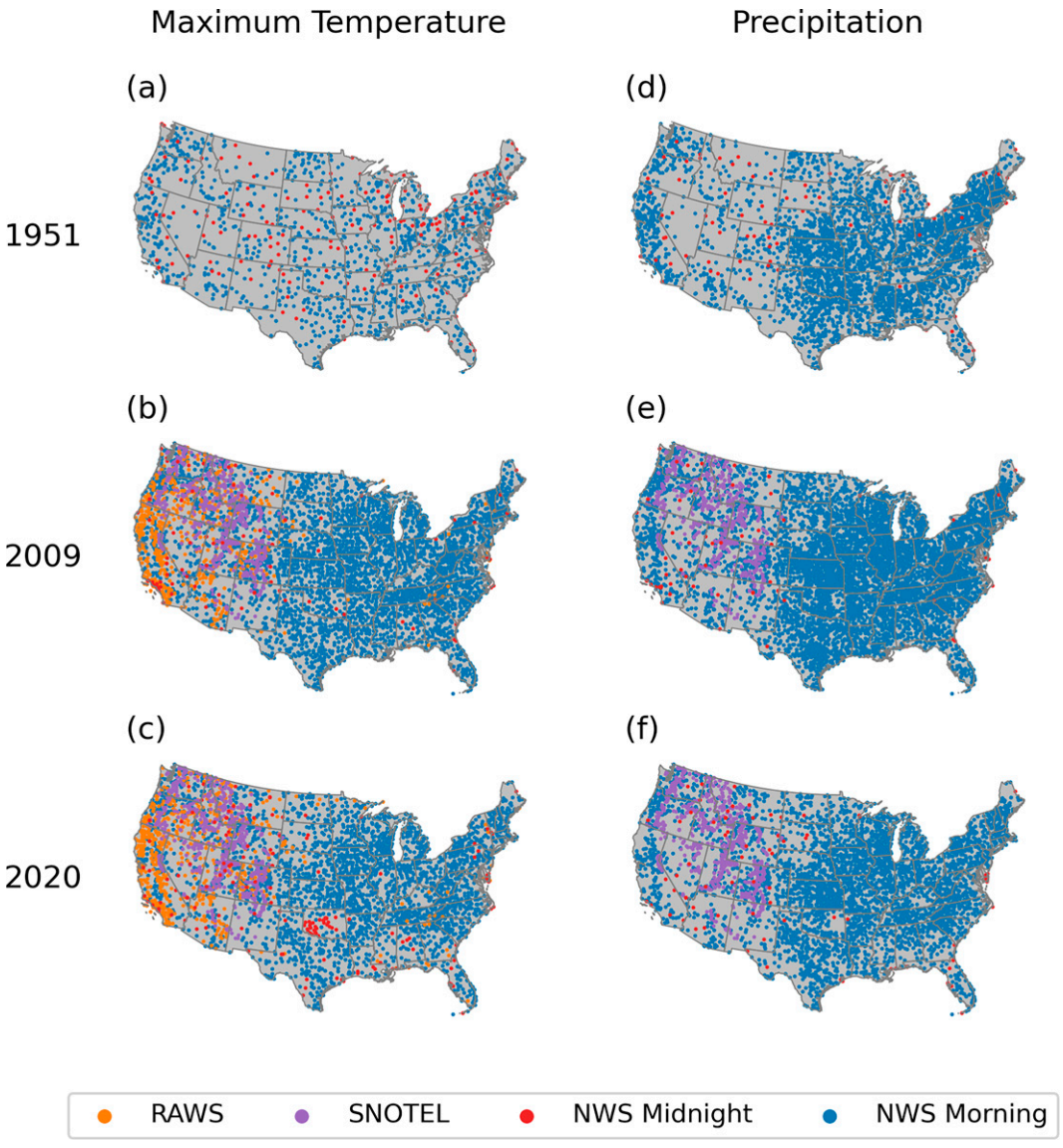

FIG. 2. Evolution of the (left) temperature (represented by Tmax) and (right) precipitation networks over the span of the nClimGrid-Daily dataset. Maps show the locations and types of observations used for (a),(d) 1 Jan 1951, the first date analyzed; (b),(e) 6 Nov 2009, the day with the largest number of input observations; and (c),(f) 31 Dec 2020, the last day analyzed in this paper. Colored circles represent NWS morning (blue), NWS midnight (red), SNOTEL (purple), and RAWS (orange) stations. The total numbers of stations shown are 1290, 4316, and 4316 for temperature in (a)–(c), respectively, and 3372, 6292, and 4692 for Prcp in (d)–(f).

3. Interpolation approach

The data selection criteria described in section 2 were applied separately to Tmax, Tmin, and Prcp observations for every day since 1 January 1951. Using the TPSS method together with several geographical predictor variables, the values chosen for each day and variable were then interpolated to a regular latitude–longitude grid that has a resolution of 1/24° and covers the CONUS land areas within the domain of 24°–52°N, 65°–130°W. Each resulting gridded field is assigned to the date of the morning observations in the corresponding set of input data and approximately represents conditions during the 24 h ending in the early morning of that date. The TPSS method is a generalized form of multivariate linear regression in which the degree of smoothness of the fitted function is determined automatically from the data by minimizing a measure of predictive error of the fitted surface. The implementation of this method for nClimGrid-Daily is based on the approach of Hutchinson (2007) and utilizes many of the same predictor variables as Vose et al. (2014). Vose et al., however, used TPSS to interpolate climatological means of monthly temperature and Prcp as part of the construction of nClimGrid-Monthly, whereas for

the creation of nClimGrid-Daily, TPSS was applied directly to the daily observations.

In preparation for the interpolation, values of six predictor variables were generated both at the grid points within the domain of the CONUS and at the locations of the observing stations. The predictor variables are described briefly here, while more specific definitions and relevant derivation procedures and data sources are detailed in Vose et al. (2014) and references therein. The three commonly used predictors of latitude, longitude, and elevation inform the interpolation of all three data variables. For Tmax and Tmin, an additional coastal influence index simulates the moderating effect of the oceans and Great Lakes as a function of the distance and topographic separation from the nearest coastline. For Prcp, two slope-aspect indices are included to model the impacts of exposure in the east–west and north–south direction. Sensitivity tests confirmed the findings of earlier studies (Hutchinson 1998b; Vose et al. 2014) that the addition of the coastal influence indicator for temperature and the slope/aspect indicators for precipitation reduces the interpolation errors, while other combinations of these predictor variables yielded less favorable results.

With the data and predictors in place, the creation of each gridded field requires the following three steps: 1) subsampling the input data, 2) fitting a surface, or function, to the subsampled data, and 3) using the fitted function to generate the final gridded field. Following Hutchinson (2007), the "generalized cross validation" (GCV; Craven and Wahba 1979) is used to assess the predictive error of each fitted surface.

The purpose of the subsampling step is to both decrease the overall processing time and eliminate the possibility of overfitting in areas with dense data coverage (Hutchinson 1998a, 2007). For each gridded field, the lesser of 4500 and 50% of the data points available are selected automatically as the subset of points through which the spline surface is fit. The algorithm selects these so-called knots according to the uniqueness of their predictor values. The setting for the number of knots was chosen based on sensitivity tests with several settings used in previous studies (Hutchinson 1998a, 2007; Vose et al. 2014). For example, when the entire three-step ANUSPLIN algorithm was applied to an arbitrarily chosen 2-yr sample of the input data (1 July 2009–30 June 2011), the eventually chosen setting of the lesser of 4500 and 50% of the number of input observations yielded a 3.3-times-faster processing time compared to Vose et al.'s setting of 75% of the input points. However, the GCV values associated with the two runs were within 1% of each other, indicating that there was no appreciable difference in the accuracy of the gridpoint estimates.

Next, a partial thin plate smoothing spline surface, constructed from the chosen set of knots, is fit to the input data, relying on the GCV as the measure for minimizing the predictive error. In the case of Prcp, the square roots of the observed values, rather than the raw values, are interpolated in order to dampen the effects of the extreme positive skewness of this variable (Hutchinson 1998a,b).

Finally, actual gridpoint estimates are derived from the spatially continuous spline function using the grids of the relevant predictors as the independent variables. For Prcp, the inverse of the square root transformation is also applied, so that the gridpoint values are presented in the original measurement units of the observations.

4. Creation of final temperature fields

Once the data have been interpolated to a regular grid, some postinterpolation processing steps are taken in an effort to improve the utility of the gridded fields. These steps differ between temperature, covered in this section, and Prcp, covered in section 5.

For temperature, the postinterpolation steps resolve any internal inconsistencies of the daily gridpoint values and establish consistency with nClimGrid-Monthly's corresponding monthly means.

a. Adjustments for internal inconsistencies

Since interpolation is applied to each day and variable separately, a day's Tmax and Tmin fields may contain grid points where the estimated Tmax is colder than the corresponding Tmin estimate. In addition, a grid point's Tmax on one day may be colder than Tmin on the previous day, or Tmin may be warmer than the prior day's Tmax. In correctly reported observations, none of these scenarios is possible because Tmax and Tmin represent the highest and lowest temperatures reported during a continuous sequence of 24-h periods, implying that the temperature ranges on consecutive days must always touch or overlap (Durre et al. 2010). In the interpolated fields, such inconsistencies may be present as a result of reporting errors in the observations, interpolation across strong temperature gradients, or the use of a mix of morning and midnight observations.

To achieve consistency between Tmax and Tmin, the following three types of empirical adjustments are applied to each day's Tmax and Tmin fields.

1) For each gridpoint day on which Tmax $<$ Tmin, both temperatures are replaced with their average. For example, if Tmax is 22.1°C and Tmin is 22.3°C, both values are replaced by 22.2°C.
2) For each gridpoint day on which Tmax is lower than the previous day's Tmin, Tmax is replaced by that previous day's Tmin. For example, if yesterday's Tmin is 10.0°C, and today's Tmax is 9.8°C, then today's Tmax is raised to 10.0°C. While it may seem more intuitive to replace both temperatures that are part of an interday inconsistency with their average, that approach turned out not to be practical at the transition between months, particularly during operational processing.
3) Analogously, when Tmin is warmer than the previous day's Tmax, Tmin is replaced with the previous day's Tmax.

The frequency of these three types of inconsistencies depends on the magnitude of the interpolation error compared to the spatial and temporal variability and therefore varies geographically, seasonally, and from one day to the next. During 1951–2020, the percentage of grid points affected by any of these inconsistencies averaged 0.03% day^{-1}, varying from

0.002% in July to 0.11% in January. The average magnitude of the inconsistencies is 0.65°C over the entire period and is considerably higher before the 1990s (0.87°C) than from 1990 onward (0.45°C), possibly owing to the widespread availability of SNOTEL and RAWS observations which tend to improve temperature estimates in areas with complex topography during the last 30 years of the record.

b. *Alignment with nClimGrid-Monthly*

In the second postinterpolation step, the daily temperatures for each grid point and month are adjusted to bring their monthly means in line with the corresponding values in nClimGrid-Monthly (Vose et al. 2014). nClimGrid-Monthly extends back to 1895 and therefore overlaps with the full period of record of nClimGrid-Daily. Since nClimGrid-Monthly is based on temperatures that have been adjusted for temporal inhomogeneities resulting from instrument and observing biases (Menne and Williams 2009), this alignment step not only achieves consistency between the monthly and daily gridded datasets, but also incorporates the monthly mean homogeneity adjustments into nClimGrid-Daily. The incorporation of these adjustments increases the temporal homogeneity of the daily gridded temperature fields with respect to their monthly means, but is not capable of addressing any differential effects that artificial inhomogeneities may have on the tails of the frequency distribution of temperatures. Accounting for such effects would require the application of daily temperature adjustments which are presently not available for U.S. data.

The alignment with nClimGrid-Monthly is performed for each variable (Tmax and Tmin), grid point, and month separately. The required adjustment is equal to the difference between the mean of the month's daily temperatures and the corresponding nClimGrid-Monthly value. This adjustment, which is positive when the daily values average to be warmer than nClimGrid-Monthly, is then subtracted from each of the daily temperatures in the month, such that their mean matches nClimGrid-Monthly.

When the adjustment is large compared to a day's diurnal temperature range (Tmax − Tmin), the alignment step can create new Tmax − Tmin inconsistencies. To mitigate this effect, an algorithm was developed that iteratively checks for inconsistencies in the initially adjusted fields and applies additional adjustments if needed until no further inconsistencies are found. Specifically, for each month, the algorithm has the following steps.

1) Apply the process for identifying and remediating same-day and interday inconsistencies that is described in section 4a to the pair of Tmax and Tmin fields that have been aligned with nClimGrid-Monthly.
2) If no new inconsistencies were found in step 1, no further action is needed. Otherwise, at each grid point, and for Tmax and Tmin separately, record the days on which adjustments were made as well as the sum of all adjustments made in the month.
3) For each grid point and variable where an additional adjustment was made in step 1, adjust the temperatures on the remaining days to restore equality with nClimGrid-Monthly's corresponding monthly mean. For Tmin, which is always lowered to eliminate an inconsistency, this means that the remaining days' values are raised by an offset that is equal to the sum of all Tmin adjustments made in step 1, divided by the number of previously unadjusted days. For Tmax, which is always raised to remediate inconsistencies, the absolute value of the sum of Tmax adjustments is used to determine the amount by which temperatures on previously unadjusted days are decreased.
4) Return to step 1 above to determine if additional inconsistencies were created by the realignment adjustments made in step 3.

For example, consider a hypothetical 30-day month with 2 days on which the aligned Tmax is 1°C lower than the aligned Tmin. These inconsistencies are eliminated by raising Tmax and lowering Tmin each by 0.5°C on those 2 days. As a result, the monthly means of the daily Tmax and Tmin change by 1/30°, rendering them inconsistent with nClimGrid-Monthly again. To restore equality with the monthly values, Tmax and Tmin on the remaining 28 days must each be readjusted in the opposite direction by 1/28°, i.e., 1/28 of the sum of the readjustments made on the inconsistent day.

5. Creation of the final precipitation fields

For Prcp, the postinterpolation steps remove spurious nonzero totals and establish consistency with the monthly totals found in nClimGrid-Monthly.

a. *Masking according to precipitation occurrence*

Point observations of daily precipitation across the CONUS typically consist of mostly zeros interspersed with areas of nonzero amounts of varying magnitudes. The smoothing effect of the spline surface, however, tends to result in an interpolated field of mostly nonzero values. This can be seen in Fig. 3a where there are numerous dry stations and Fig. 3b where TPSS has interpolated rainfall in the region around these dry stations. On an average day during 1951–2020 across CONUS, 73.4% of the input station observations reported no precipitation, whereas only 0.13% of the TPSS-interpolated gridpoint Prcp estimates round to a value of 0.00 mm. Consequently, an additional step was needed to restore the representation of dry areas in the final gridded Prcp fields.

To accomplish this, each gridded Prcp field was masked using an approach that builds upon that of Hutchinson et al. (2009), who used TPSS to interpolate a binary precipitation occurrence indicator to the same grid to which Prcp was interpolated and then set to zero all amounts at grid points where the estimated occurrence was below 0.5. In the nClimGrid-Daily masking approach, summarized in Table 3, two fields of occurrence indicators were used, one that was interpolated with TPSS and one based on the Willmott et al. (1985) implementation of inverse distance weighting (IDW) on a spherical surface. Interpolated nonzero Prcp values were set to zero at each grid point where the TPSS-based occurrence value was less than 0.4 and the IDW-based value was less than 0.9. These

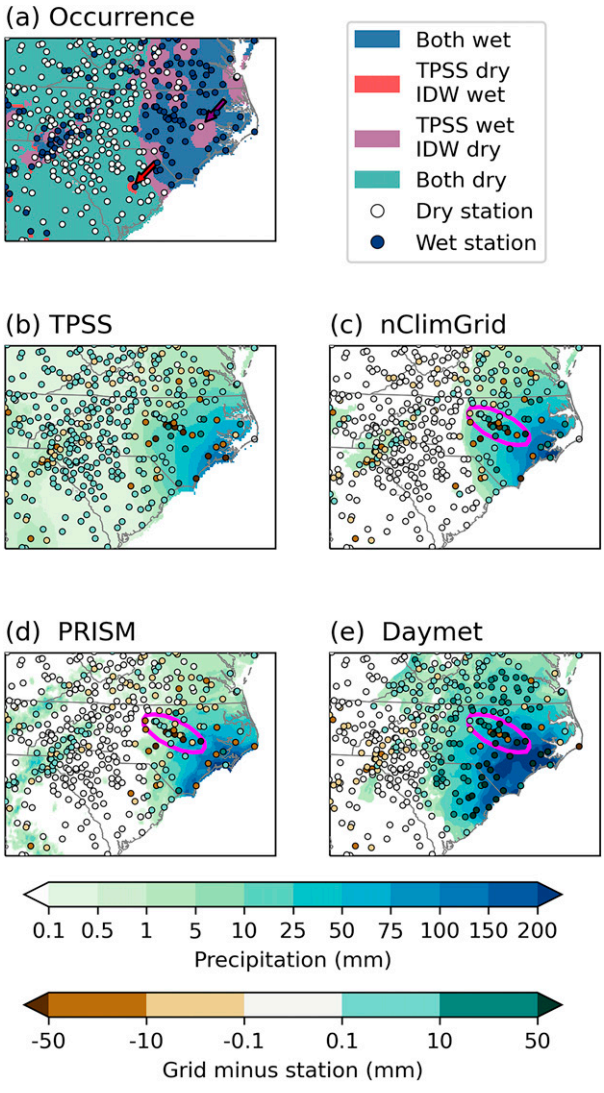

FIG. 3. Example Prcp fields during the passage of Hurricane Florence on 14 Sep 2018. (a) Occurrence of nonzero Prcp at each station and for each combination of the TPSS- and IDW-interpolated occurrence indicators. (b) Gridded Prcp from the original unadjusted TPSS interpolation, (c) the final nClimGrid-Daily field, (d) PRISM, and (e) Daymet. In (a), blue (white) circles identify stations reporting Prcp amounts greater than zero (equal to zero). In (b)–(e), colored circles represent the bias of the nearest grid point relative to each observed value. The arrows in (a) and magenta ellipse in (b)–(e) highlight locations mentioned in the text. Note that the magenta ellipse discussion is found in section 6b.

thresholds were selected after evaluating the performance of a wide range of possible values when applied to a 5-yr (2010–14) sample of the input data. The performance evaluation was conducted quantitatively via statistical comparisons of the *observed* distributions of precipitation days to corresponding *estimated* distributions at the respective nearest grid points. Additionally, a qualitative visual comparison of the masked Prcp fields during a few significant storms to the spatial patterns indicated by the input data, radar observations, and PRISM.

Over the 1951–2020 period, the masking process increased the average proportion of grid points with zeros in a daily field to 73.8%, a value that is close to that found in the observations. Among the values that are replaced with zero, 97.8% are below the widely used "wet-day" threshold of 1 mm. The IDW-interpolated occurrence indicator complements the TPSS-based indicator in that IDW is more likely to capture small-scale observed precipitation events that TPSS smooth out, while TPSS produce more accurate estimates at grid points distant from observations (Jarvis and Stuart 2001b; Hofstra et al. 2009; Wagner et al. 2012; Herrera et al. 2019).

The combined effects of the two occurrence indicators are illustrated in Fig. 3a by way of a sample day during the passage of Hurricane Florence over North Carolina in 2018. In most cases in which a gridpoint value is set to zero, both thresholds trigger the masking decision (teal shading). However, there are also areas where the benefit of each indicator is apparent. For example, the use of the IDW-based threshold allows for the preservation of the isolated rain events at two stations in central South Carolina (red arrow in Fig. 3a), which do not trigger the TPSS-based threshold (red shading). On the other hand, the TPSS-based occurrence threshold retains the significant rainfall in eastern North Carolina where the IDW-based threshold is not exceeded (purple shading) due to several apparently erroneous reports of no precipitation in their midst (e.g., purple arrow in Fig. 3a).

b. *Alignment with nClimGrid-Monthly*

Following the masking step, the Prcp fields were adjusted, so that their monthly totals matched the corresponding nClimGrid-Monthly values. Unlike in the case of temperature, consistency with nClimGrid-Monthly is not expected to improve the homogeneity of the daily gridded fields because the monthly Prcp time series that serve as input to nClimGrid-Monthly were not homogeneity adjusted. Nevertheless, as noted by Daly et al. (2021), consistency between the different time scales allows users to take advantage of the complementary daily and monthly products as appropriate for their applications.

Given the positive skewness of the frequency distribution of precipitation, a multiplicative scaling factor was used rather than the additive adjustment employed for temperature. For each month and grid point, the daily Prcp values were summed to form a monthly total. Each nonzero daily value was then multiplied by the ratio of the corresponding nClimGrid-Monthly value to that monthly sum. When the final values were written out to the nearest hundredth of a millimeter, scaled values less than 0.005 mm were written as zeros.

6. Validation

Previous studies showed that the accuracy of gridded data for the CONUS is primarily a function of the interpolation error that results from gaps in the spatial distribution of stations and from the chosen interpolation method's handling of strong gradients such as those induced by specific weather events or by the presence of topography (DeGaetano and Belcher 2007; Diluzio et al. 2008; Gervais et al. 2014; Daly et al. 2021;

TABLE 3. Steps involved in the process of masking an initially interpolated field of Prcp values in an effort to remove spurious nonzero values introduced by the smoothing effect of TPSS. The abbreviations occ_TPSS and occ_IDW stand for a grid point's TPSS-based and IDW-based occurrence values, respectively. A trace is a nonzero precipitation amount that is too small to measure, i.e., <0.13 mm (<0.005 in.) in U.S. observations. See section 5a for details.

Step No.	Description	Output	Notes
1	Generate set of occurrences at stations	0 when Prcp is 0 or trace, 1 when Prcp > trace	Use same input data as for Prcp interpolation
2a	Interpolate occurrences using TPSS	Grid of real numbers between 0.00 and 1.00 (occ_TPSS)	Same predictors as for Prcp; no square root transformation; set negative estimates to 0, those >1 to 1.00
2b	Also interpolate occurrences using IDW on a sphere	Grid of real numbers between 0.00 and 1.00 (occ_IDW)	Use Willmott et al. (1985) approach
3	Set gridpoint Prcp to 0 when occ_TPSS < 0.4 and occ_IDW < 0.9	Grid of Prcp amounts with realistic proportion of zero	See text for rationale for selecting these thresholds

Thornton et al. 2021). A variety of steps were taken to assess the performance of nClimGrid-Daily qualitatively and quantitatively in these respects. The key results from these assessments are presented below.

a. Validation approach

The qualitative assessments included the examination of the spatial patterns of the gridded fields in relation to the corresponding patterns in the input data on days of significant weather events. To complement these evaluations, the gridded fields from two other prominent datasets were also compared to the same set of observations on these days. These comparative assessments provide additional information on the degree to which interpolation techniques in general can be expected to accurately represent large spatial variability. The 4-km-resolution daily fields from PRISM (Diluzio et al. 2008) and the 1-km-resolution fields from Daymet version 4 (Thornton et al. 2021) were used for these comparisons since they have similar spatial resolutions but are based on different data selection and interpolation approaches compared to nClimGrid-Daily.

For the quantitative assessment, the magnitude and variability of the interpolation error is best characterized by spatial and temporal analyses of the differences between observations and collocated unadjusted TPSS estimates. Such statistics were generated in the form of leave-one-out cross-validation results during the application of the TPSS method. For each day, variable, and input data point, the Hutchinson (2007) TPSS procedure produces an error estimate by removing the observation, fitting a surface through the remaining data, and estimating the value and corresponding residual at the location of the withheld point. Maps of these residuals depict the spatial distribution of the interpolation error, and the root-mean-square error (RMSE) of the estimate − observation residuals across all available input data points provides a measure of the accuracy of the field as a whole.

b. Spatial distribution of temperature errors

Figure 4 presents a qualitative example of how nClimGrid-Daily and other gridded datasets perform during a cold-air outbreak over the Rocky Mountains and High Plains on 3 February 1989. This example illustrates the various factors that may contribute to the presence of larger errors in the mountainous regions of the West. In the early morning hours of the previous day, 2 February 1989, a strong cold front passed through this region, resulting in 1-h temperature drops exceeding 15°C and some further decreases until the morning of the following day. As shown in Fig. 4g, the region is characterized by mountain ranges, valleys, and plateaus, and the input data for the 3 February nClimGrid-Daily grids are a mix of readings taken in the morning of 3 February and at the next-earlier midnight on 2 February. Thus, the unusually large spatial variability in the observations can be attributed not only to local topographic and climatic factors, but also to location-to-location differences in the timing of the frontal passage in relation to each station's 24-h observing period.

Despite this significant variability, the interpolated nClimGrid-Daily fields in Figs. 4a and 4d largely agree with the pattern of station temperatures. In areas of limited station coverage, nClimGrid-Daily produces reasonable variations with elevation, such as the cooler temperatures along the Uncompahgre Plateau of western Colorado (black oval). In regions with isolated outliers in station temperatures, however, the interpolated Tmin and Tmax fields tend to be more reflective of the conditions at surrounding stations, smoothing out the effects of the outliers. Examples are the unusually cold Tmins along the Front Range (black wavy line in Fig. 4d) and two unusually warm Tmax values in northeastern New Mexico and southeastern Colorado (yellow arrows in Fig. 4a).

The PRISM (Figs. 4b,e) and Daymet (Figs. 4c,f) interpolation techniques also were challenged by the day's unusual temperature patterns. Like nClimGrid-Daily, PRISM and Daymet exhibit a tendency for the gridded Tmin to be warmer than the observations along the Front Range (Figs. 4e,f), with PRISM showing the largest bias. The Daymet Tmax field (Fig. 4c) exhibits large cold biases (>5°C) relative to many stations and is colder than PRISM and nClimGrid-Daily over much of the region. Overall, the gridpoint-station differences appear to be more randomly distributed for nClimGrid-Daily than for the other two datasets. Together, the panels of Fig. 4 illustrate the uncertainties that can be associated with interpolating unevenly distributed observations of highly variable temperatures to a high-resolution regular grid (Behnke et al. 2016; Walton and Hall 2018).

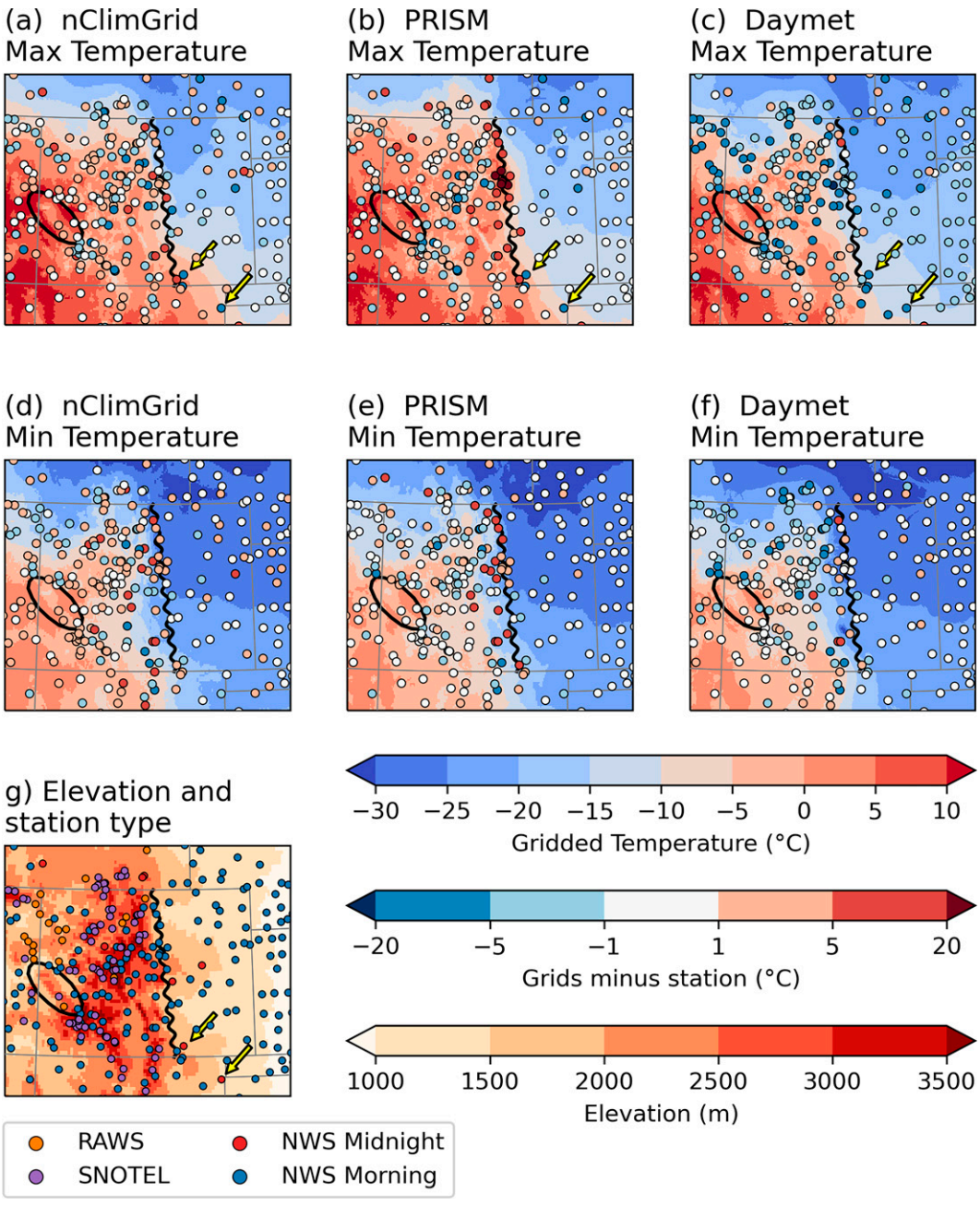

FIG. 4. Example gridded (a)–(c) Tmax and (d)–(f) Tmin for the Rocky Mountains and High Plains region on 3 Feb 1989. (a),(d) The final nClimGrid-Daily. (b),(e) PRISM. (c),(f) Daymet. (g) Elevation and station type for reference. In (a)–(f), colored circles represent the bias of the nearest grid point relative to each observed value. The wavy black line, black oval, and yellow arrows highlight locations mentioned in the text.

Figure 5 shows CONUS-wide maps of long-term averages of mean absolute differences (MAD) and biases over the years 1991–2020, the period in which the NWS, SNOTEL, and RAWS networks were all in full operation. The MAD at each station is computed by finding the absolute difference between the TPSS unadjusted estimate and the station's value on every day and then taking the mean over all days in the 1991–2020 period. The bias is calculated analogously, but without taking the absolute value of each daily difference. Since the bias is defined as the estimate − observation difference, a positive value reflects a warm bias in the estimates.

The median of the Tmax MAD values across all stations (Fig. 5a) is about 1°C. Almost 75% of the stations have a value less than 1.3°C and are spread across the entire country. The higher MAD values are sparsely distributed in mountainous regions across the West. The median MAD value for

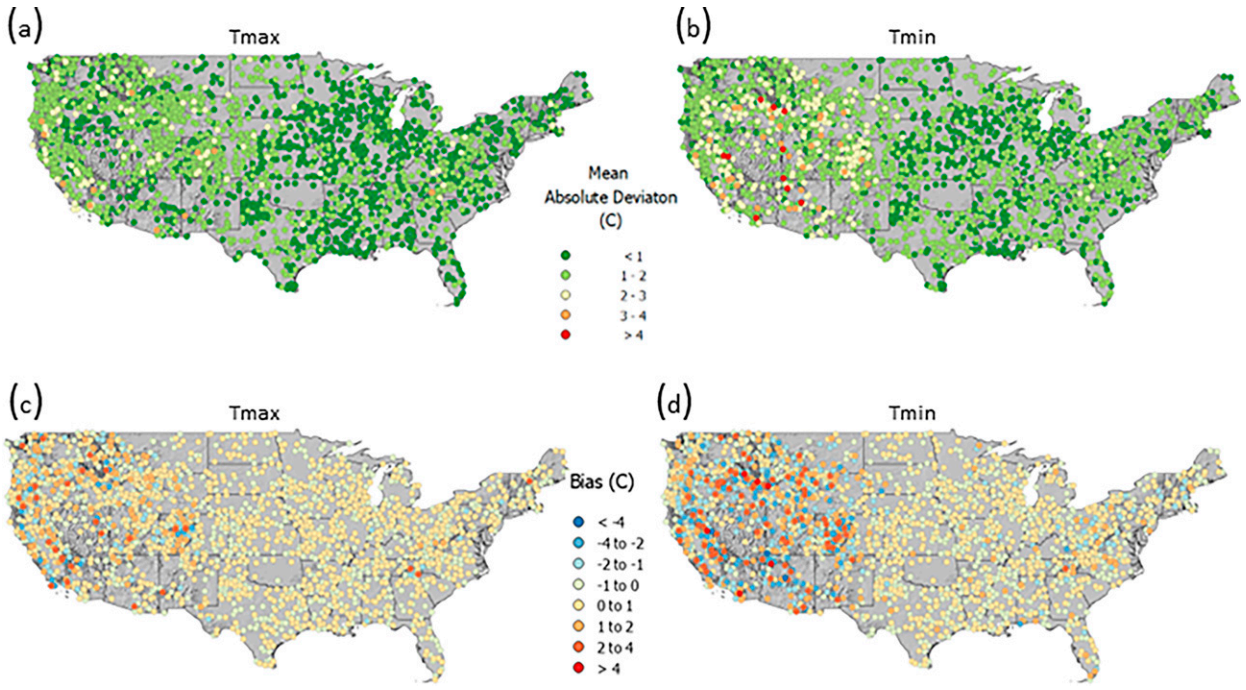

FIG. 5. Maps of (a),(b) mean absolute differences and (c),(d) biases between unadjusted TPSS estimates and collocated (a),(c) Tmax and (b),(d) Tmin observations for the period from 1 Jan 1991 to 31 Dec 2020. Totals of 2463 Tmax and 2416 Tmin stations with data on at least 80% of the possible days are shown. In (c) and (d), a positive difference indicates that the TPSS estimate is greater than the observed value.

Tmin (Fig. 5b) is also about 1°C. Of the 2416 Tmin stations, almost 75% have a MAD value less than 1.5°C, and these are spread throughout the country. The remaining stations with higher MAD values are in the mountainous regions of the West. The median bias of Tmax (Fig. 5c) is about 0°C. Almost 90% of the stations have bias values of ±1°C and are located throughout the country. Most of the stations with higher bias values are in the Sierra Nevada of California and the mountainous regions of Idaho and Colorado. Like the Tmax biases, the Tmin bias for this set of stations is close to 0°C. Almost 75% have a bias of ±1°C and are distributed throughout the country. The stations with larger Tmin bias values are in the Intermountain West and the mountainous areas of California.

c. *Spatial distribution of precipitation errors*

Figure 6 shows median absolute deviations and bias ratios for the unadjusted TPSS Prcp estimates for "wet days" spanning the 1991–2020 period. A wet day is defined as a day on which a station has at least 1 mm of precipitation. There were 3233 stations that met the 80% completeness criterion during this period. The median absolute deviation, shown in Fig. 6a, is similar to the MAD, except that the nonparametric median

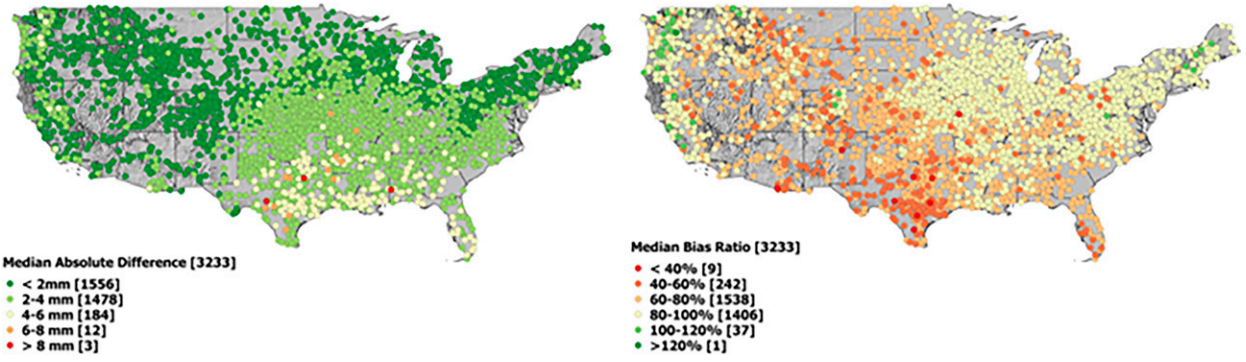

FIG. 6. Comparisons between unadjusted TPSS estimates of Prcp and collocated observations for the period from 1 Jan 1991 to 31 Dec 2020 for wet days, i.e., days with observed Prcp ≥ 1 mm. (a) Median absolute estimate − observation differences (in mm). (b) Median estimate/observation ratios (%). The 3233 stations shown have data on at least 80% of the possible days.

is used instead of the mean due to the variety of Prcp distributions across the CONUS. Half of the values in Fig. 6a are below 2 mm and 75% are below 3 mm. The prevalence of these relatively small error values is consistent with the fact that, at most locations, the majority of daily Prcp amounts is also quite small. Larger absolute errors are more common when Prcp amounts are also large. For example, the highest median absolute deviation values roughly correspond to areas of high average Prcp, especially in the southern United States. Lower error values are found in the generally drier West and across the northern tier of states.

The bias ratio, displayed in Fig. 6b, is calculated by dividing the estimated value by the observed value and multiplying by 100% at each station on each wet day. All the percentages for a station are ranked, and the median bias ratio is determined. Virtually all of the stations in Fig. 6b have a bias ratio less than 100%, indicating that the unadjusted TPSS has a dry bias for Prcp stations with the driest bias extend from Texas northwestward through the mountainous West. Most of the stations with a wet bias are in California, Oregon, and Washington. The predominance of negative biases in the estimates is expected from the smoothing effect of the TPSS method and is characteristic of many gridded precipitation datasets (e.g., Gervais et al. 2014). The comparatively fewer positive differences that are scattered across the western United States are likely to be related to the combined effects of isolated precipitation events, sparse observations, and complex topography that complicate the generation of reliable spline surfaces. In the case of nClimGrid-Daily, the alignment with nClimGrid-Monthly tends to reduce the degree of underestimation resulting from the TPSS interpolation. In the Hurricane Florence example, for instance, the raw TPSS estimates (Fig. 3b) show large dry biases compared to some of the heaviest rainfall amounts, and the adjustments made as part of the alignment step more than compensate for these biases and actually result in overestimates (Fig. 3c).

Figure 3c provides a case study for the Hurricane Florence example referenced in section 5. Generally, the interpolated field reflects the spatial pattern of the observations. Significant differences appear primarily around isolated dry or wet stations and in the Raleigh–Durham area where station-to-station variability in precipitation amounts was particularly large (magenta ellipse in Fig. 3c). The overall precipitation pattern is similar in PRISM (Fig. 3d). However, Daymet is significantly wetter than the other two datasets with both more widespread maximum precipitation and a broader area with values > 0.1 mm.

d. Temporal variations in interpolation errors

Time series of monthly means of the whole-field RMSE for 1951–2020 are displayed in Fig. 7. Over nClimGrid-Daily's period of record, the overall Tmax RMSE values decrease from between 0.75° and 1.10°C in the 1950s to a range of 0.6°–0.9°C in the 2010s, a period during which the number of input data points more than doubles (Fig. 1). Tmin errors vary from ~0.7° to ~1.2°C throughout the period and appear to be less closely related to the total number of stations than the RMSEs for Tmax. RMSEs for Prcp primarily lie between ~0.2 and ~0.35 mm, with a narrower range and larger cold season errors in the latter half of the record.

From Figs. 1, 2, and 7 it appears that several factors influence the whole-field RMSE of the estimate − observation residuals. As documented in previous studies (e.g., Ensor and Robeson 2008; Gervais et al. 2014; Daly et al. 2021; Thornton et al. 2021), while an increase in station density is generally expected to lower the RMSE, a greater mix of observation times and a larger proportion of stations in areas where interpolation is challenging can have the opposite effect. These counteracting effects may be reflected in the increase in RMSE during the increase in SNOTEL and RAWS stations in the 1980s.

7. Climate monitoring applications

The analyses of the previous section indicate that significant uncertainties are associated with estimates for individual days at grid points, particularly in the context of significant spatial and temporal variability. They further show that, despite these uncertainties, which are common among daily gridded datasets in general, the nClimGrid-Daily fields reflect the overall spatial patterns in Tmax, Tmin, and Prcp. It can therefore be expected that nClimGrid-Daily is suitable for its primary purpose of supporting climate monitoring applications at regional to national scales which typically require the spatial and/or temporal aggregation of gridpoint estimates. Two such applications are presented in this section, along with assessments of the uncertainty associated with the respective results.

a. Climatological areal percentages

A common climate monitoring application of high-resolution daily gridded fields is the computation of areal percentages of climatic conditions, expressed as threshold exceedances, that are significant to the agricultural, health, tourism, infrastructure, or other sectors. To determine how anomalous current conditions are across CONUS as a whole, such areal percentages for a recent period are typically compared to corresponding climatological reference values. To illustrate the performance of nClimGrid-Daily in this context, some climatological reference values for several types of threshold exceedances were calculated from nClimGrid-Daily and compared to those derived from the widely used PRISM product (Diluzio et al. 2008).

Figure 8 shows long-term monthly mean areal percentages across CONUS of several variable–threshold combinations for the period 1981–2018 as calculated from nClimGrid-Daily (blue lines) and from the PRISM dataset (orange lines). For each day in the period, grid cells were identified that satisfied each combination of variable and threshold condition. The results were aggregated into percent areas, using the cosine of the latitude of each grid cell's centroid, and presented as 1981–2018 monthly means to show the typical areal coverage of the chosen conditions.

The primary methodological differences between nClimGrid-Daily and PRISM are the use of different interpolation techniques and PRISM's inclusion of additional sources of information (e.g., radar) in the modern era that both improve the quality of

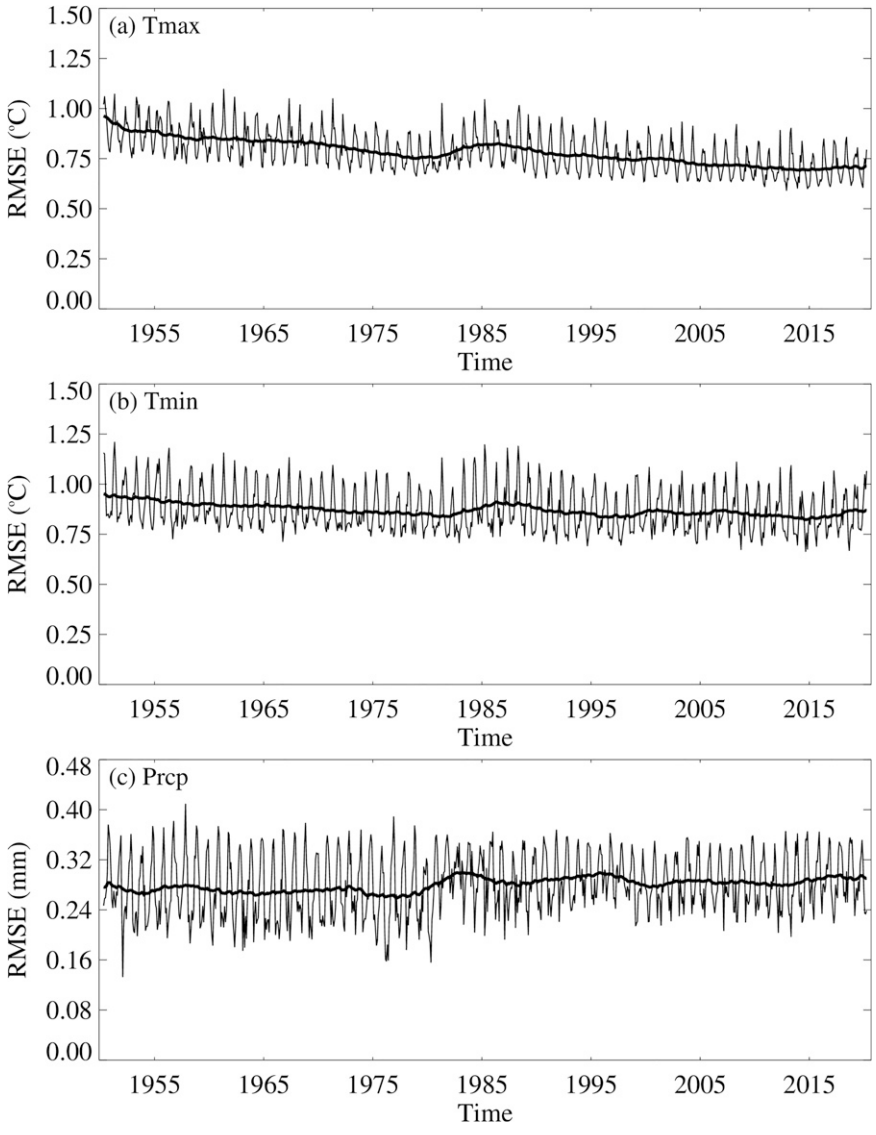

FIG. 7. Monthly mean root-mean-square interpolation errors between January 1951 and December 2020 for (a) Tmax, (b) Tmin, and (c) Prcp. Values are smoothed with a 49-month running mean to emphasize longer-term variations. See text for additional explanation.

individual gridded fields and may introduce temporal inhomogeneities into the record. Despite these different approaches, the climatological areal percentages calculated from nClimGrid-Daily and PRISM exhibit reasonably close agreement for the example Tmax, Tmin, and Prcp parameters shown in Fig. 8. For Tmax and Tmin, both products exhibit large annual cycles, with very good agreement in all months (Figs. 8a–d). For example, the area with Tmax exceeding 35°C peaks at 17% in July and drops to 0% in January (Fig. 8b), while the area with Tmin below 0°C decreases from ~76% in January to <0.1% in July (Fig. 8d). For portions of CONUS extending west from 105°W (dashed lines in Fig. 8), an area characterized by topographic and climatic conditions that are particularly challenging for interpolation algorithms, the Tmax and Tmin statistics based on nClimGrid-Daily and PRISM are in similarly good agreement and exhibit annual cycles that closely follow their CONUS-wide counterparts. Overall, the mean absolute differences in monthly areal percentages shown in Figs. 8a–d vary from ~0.1% to ~0.9% across months and threshold categories, whereas the peak absolute difference for any particular monthly comparison is ~2.3%.

The percentage of CONUS with Prcp ≥ 2.5 mm, as calculated from nClimGrid-Daily, reaches its maximum of 23% in June and dips to 15% in January and 16% in October, while percentages based on PRISM differ by up to 2% (Fig. 8e). For the threshold of 25 mm (Fig. 8f), the climatological percent area varies between 1.4% and 1.9% during the year in nClimGrid-Daily, with differences of up to 0.2% between the two products. In the area west of 105°W, with its extremely

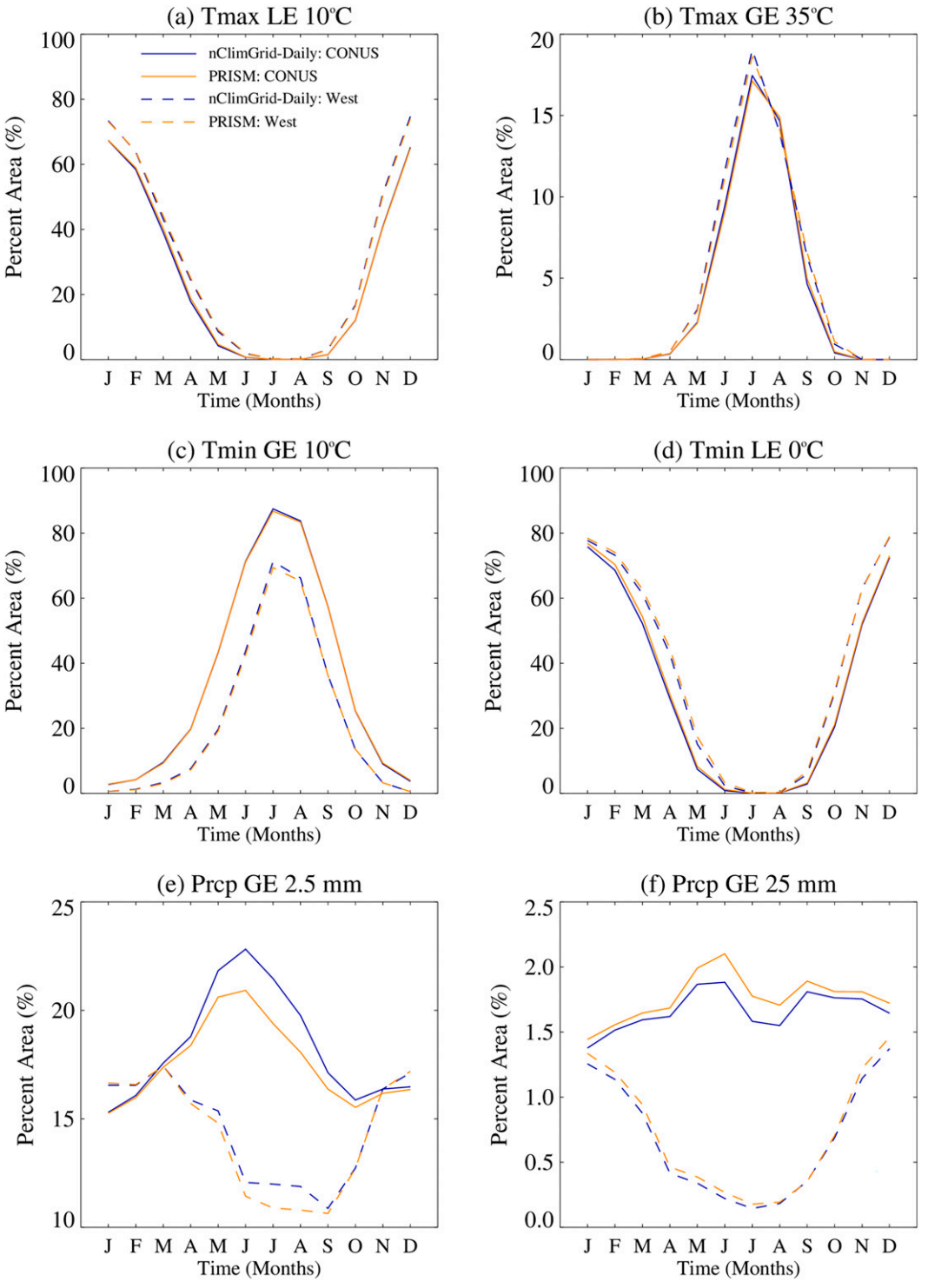

FIG. 8. Mean monthly areal percentages of the CONUS (solid lines) and the portion of CONUS extending westward from 105°W (dashed lines) that experienced (a) Tmax ≤ 10°C, (b) Tmax ≥ 35°C, (c) Tmin ≥ 10°C, (d) Tmin ≤ 0°C, (e) Prcp ≥ 2.5 mm, and (f) Prcp ≥ 25 mm. Mean percentages are computed over the 1981–2018 period of record from nClimGrid-Daily (blue) and PRISM (orange).

dry summers and comparatively wet winters, the Prcp statistics match more closely than in the CONUS-wide result.

Overall, the results shown in Fig. 8 demonstrate that in terms of climatological means of aerial percentages for various threshold exceedances, nClimGrid-Daily is in good agreement with the PRISM product. This is true both for CONUS as a whole and for the more topographically complex West.

b. *Trends in extremes*

A source of uncertainty that may impact analyses of long-term climate variability based on nClimGrid-Daily is the temporal variation in the spatial coverage of the underlying observations. To evaluate the significance of this uncertainty in the context of a likely application, trends in three extreme metrics were compared to those calculated from a constant-network version of nClimGrid-Daily.

The constant-network set of gridded fields was created by applying the nClimGrid-Daily gridding process described in sections 3–5 to observations from a subset of 250 relatively evenly distributed stations with rather complete records during the years 1981–2015. Compared to longer periods, this 35-yr period provided a reasonable distribution of suitable station time series. The records of 240 of these stations were at least 95% complete with observations from a single (morning or midnight) observation time, while the remaining 10, with ≥85% completeness, filled in spatial gaps in the Intermountain West.

Figure 9 shows the 1981–2015 trends by grid cell for three common climate extreme metrics: the warmest Tmax, coldest Tmin, and highest Prcp of the year (e.g., Caesar et al. 2006). Overall, nClimGrid-Daily's full-network trend patterns (Figs. 9a,d,g) are quite similar to those based on the constant network (Figs. 9b,e,h) and are in qualitative agreement with results from previous studies (e.g., Donat et al. 2013; Thorne et al. 2016; Dunn et al. 2012). Despite the overall good agreement, values at individual grid points can differ significantly between the two versions. Across all grid cells, mean absolute differences average 0.13° (0.20)°C decade^{-1} for the warmest Tmax (coldest Tmin) and 1.8 mm decade^{-1} for the highest Prcp. Therefore, trends calculated from nClimGrid-Daily are best assessed on a regional to national level rather than at individual grid points.

In both versions, positive trends in the coldest Tmin extend over the vast majority of CONUS and are more pronounced than those for the warmest Tmax, which are largest in the West and in the southern Plains (Figs. 9a,d). For the wettest Prcp (Figs. 9g,h), positive (negative) trends prevail in the eastern two-thirds (western one-third) of CONUS. Only the patterns for the warmest Tmax diverge somewhat in parts of the Midwest, Northeast, and northern Great Plains, where the full network shows greater warming than the constant network. This discrepancy could be the result of the better representation of spatial variability in the full-network version. Another reason could be the greater temporal homogeneity that results from using a fixed set of stations with largely temporally consistent observation times in the constant-network version. While the Tmax and Tmin fields in both versions are constructed to be consistent with homogeneity-adjusted monthly mean temperatures (see section 4b), inhomogeneities in the frequency distribution of daily temperatures have not been addressed. Consequently, the degree of spatial coherence of trends, their physical consistency with trends in other variables, and their consistency with findings from other studies are important considerations when evaluating the fidelity of trends derived from nClimGrid-Daily.

8. Product availability and usage

To support climate and drought monitoring at a wide range of spatial scales, NCEI makes available both gridded fields and regional averages as part of nClimGrid-Daily. In addition to the variables of Tmax, Tmin, and Prcp, gridded daily mean temperature is also included as the average of the Tmax and Tmin fields. Spatial averages of all four variables are provided for the following nine types of regions within CONUS: census tracts, counties, states, U.S. climate divisions, NWS Weather Forecast Office regions, major watersheds according to Hydrologic Unit Code 1, the NCEI monitoring regions, the regions used in the Fifth U.S. National Climate Assessment, and CONUS as a whole. In most cases, a regional average was calculated as the mean of values at grid points within the region, weighted by the cosine of the latitude of each grid point. For census tracts smaller than a grid box, the value of the grid point that is closest to the coordinates of the tract's centroid was used.

The nClimGrid-Daily data begin with 1 January 1951 and extend to the most recent available day. In real time, a new day's fields and averages typically become available 2–3 days after the observation date. At that point, however, they are based on only a portion of the expected total number of observations and have not been aligned with nClimGrid-Monthly. The accuracy of the estimates improves over subsequent days and months as additional data are received and the corresponding nClimGrid-Monthly values become available. All estimates for a given month are labeled as "preliminary" until the fourth day of the subsequent month, when they can be adjusted to match the corresponding gridpoint values in the nClimGrid-Monthly product. At that same time, data for the previous two months are also reprocessed in order to incorporate any additional observations that may have been received. Reprocessing of earlier data will only occur when deemed necessary and will be accompanied by a change in the dataset version identifier. Therefore, users seeking a stable set of nClimGrid-Daily data should avoid data from the current and previous two months, and users of the real-time nClimGrid-Daily data are advised to assess the impact of using the preliminary estimates on their particular application.

As described in sections 2–5, the gridded fields were generated by 1) using TPSS to interpolate a combination of morning and midnight observations from GHCNd, 2) further processing the resulting gridded fields to improve the identification of dry grid points in the Prcp field and to ensure internal consistency between Tmax and Tmin, and 3) aligning the daily fields with those in nClimGrid-Monthly. Temporal inhomogeneities in

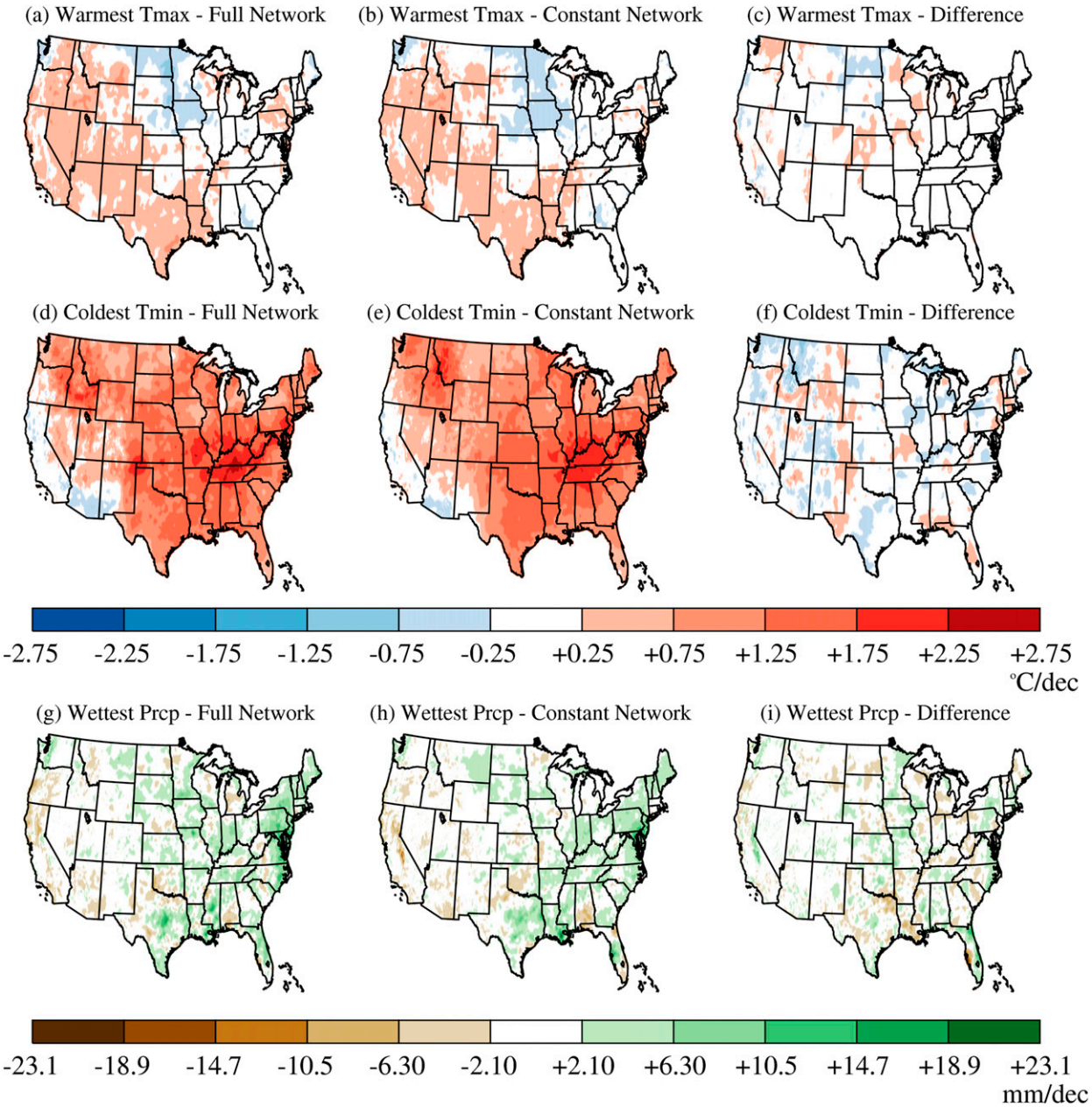

FIG. 9. Trends in (a),(b) the warmest Tmax of the year, (d),(e) coldest Tmin of the year, and (g),(h) wettest day of the year over 1981–2015 from (a),(d),(g) the full nClimGrid network and (b),(e),(h) a 250-station constant network subset. The differences in the trend computations between the full and constant networks for the (c) warmest Tmax of the year, (f) coldest Tmin of the year, and (i) wettest day of the year are also displayed. Average trends in the full (constant) network versions are 0.18°C decade^{-1} (0.44°C decade^{-1}) for the warmest Tmax, 1.00°C decade^{-1} (1.02°C decade^{-1}) for the coldest Tmin, and 1.00 mm decade^{-1} (0.86 mm decade^{-1}) for the highest Prcp.

nClimGrid-Daily are limited by restricting the observation times and station networks used as input. In the case of temperature, month-to-month inhomogeneities in the monthly mean have effectively been removed from the daily fields through the alignment with nClimGrid-Monthly. Nevertheless, users of nClimGrid-Daily are advised to use multiple quantitative and qualitative methods to assess any temporal changes found for possible nonclimatic influences (Hofstra et al. 2009; Donat et al. 2013; Vose et al. 2014; Contractor et al. 2020).

The primary purpose of this product is to support applications such as drought monitoring that require time series of spatially aggregated data. Reliance on single-day values and individual points is discouraged due to the significant uncertainty

that is inherent in such a product because of the spatial distribution of the underlying observations, differences in observation time between neighboring stations, and interpolation errors. Spatial and temporal averaging tends to reduce the effect of these uncertainties (Behnke et al. 2016). As shown by way of some examples in section 7, time series of such aggregated values as well as spatial patterns of gridpoint statistics are suitable for climatological applications such as the analysis of trends in extremes.

Acknowledgments. The authors thank Tom Burnet, a former member of the team, for his significant technical contributions to the development of the nClimGrid-Daily processing system and to the implementation of the cross-validation analysis and various other validation steps. We also thank Wendy Gross for her technical contribution and Xungang Yin for his support during the preparation of this manuscript. Finally, we appreciate the feedback from all peer reviewers. C. Schreck was supported by NOAA through the Cooperative Institute for Satellite Earth System Studies under Cooperative Agreement NA19NES4320002. This work was also partially supported by the National Integrated Drought Information System. The scientific results and conclusions, as well as any views or opinions expressed herein, are those of the authors and do not necessarily reflect those of NOAA or the Department of Commerce.

Data availability statement. The dataset described herein is version 1.0.0 of nClimGrid-Daily, which is openly available from NCEI. The full dataset citation is given in the Durre et al. (2022) reference, and various methods for accessing the data are provided at the following URL: https://www.ncei.noaa.gov/products/land-based-station/nclimgrid-daily. Data from GHCNd version 3 (Menne et al. 2012a,b) were accessed continuously throughout the development of nClimGrid-Daily during 2014–18 and continue to be accessed for daily updates of the product. Beginning with data for January 2020, each nClimGrid-Daily update includes a version file that documents which version of GHCNd was used. GHCNd is available from NCEI as cited in Menne et al. (2012a,b). The two datasets used for the validation of nClimGrid-Daily are also openly available. The 4-km gridded fields of daily temperature and precipitation from PRISM are available from the PRISM Climate Group, Oregon State University, at https://prism.oregonstate.edu, and were accessed in October 2019. Gridded fields for "Daymet: Daily Surface Weather Data on a 1-km Grid for North America, version 4" were obtained from https://doi.org/10.3334/ORNLDAAC/1840 in May 2022.

REFERENCES

Behnke, R., S. Vavrus, A. Allstadt, T. Albright, W. Thogmartin, and V. Radeloff, 2016: Evaluation of downscaled, gridded climate data for the conterminous United States. *Ecol. Appl.*, **26**, 1338–1351, https://doi.org/10.1002/15-1061.

Caesar, J., L. Alexander, and R. Vose, 2006: Large-scale changes in observed daily maximum and minimum temperatures: Creation and analysis of a new gridded data set. *J. Geophys. Res.*, **111**, D05101, https://doi.org/10.1029/2005JD006280.

Chen, M., W. Shi, P. Xie, V. B. S. Silva, V. E. Kousky, R. W. Higgins, and J. E. Janowiak, 2008: Assessing objective techniques for gauge-based analyses of global daily precipitation. *J. Geophys. Res.*, **113**, D04110, https://doi.org/10.1029/2007JD009132.

Contractor, S., and Coauthors, 2020: Rainfall Estimates on a Gridded Network (REGEN)—A global land-based gridded dataset of daily precipitation from 1950 to 2016. *Hydrol. Earth Syst. Sci.*, **24**, 919–943, https://doi.org/10.5194/hess-24-919-2020.

Craven, P., and G. Wahba, 1979: Smoothing noisy data with spline functions. *Numer. Math.*, **31**, 377–403, https://doi.org/10.1007/BF01404567.

Daly, C., W. P. Gibson, G. H. Taylor, M. K. Doggett, and J. I. Smith, 2007: Observer bias in daily precipitation measurements at United States Cooperative network stations. *Bull. Amer. Meteor. Soc.*, **88**, 899–912, https://doi.org/10.1175/BAMS-88-6-899.

——, and Coauthors, 2021: Challenges in observation-based mapping of daily precipitation across the conterminous United States. *J. Atmos. Oceanic Technol.*, **38**, 1979–1992, https://doi.org/10.1175/JTECH-D-21-0054.1.

DeGaetano, A. T., 1999: A method to infer observation time based on day-to-day temperature variations. *J. Climate*, **12**, 3443–3456, https://doi.org/10.1175/1520-0442(1999)012<3443:AMTIOT>2.0.CO;2.

——, and B. N. Belcher, 2007: Spatial interpolation of daily maximum and minimum air temperature based on meteorological model analyses and independent observations. *J. Appl. Meteor. Climatol.*, **46**, 1981–1992, https://doi.org/10.1175/2007JAMC1536.1.

Diluzio, M., G. L. Johnson, C. Daly, J. K. Eischeid, and J. G. Arnold, 2008: Constructing retrospective gridded daily precipitation and temperature datasets for the conterminous United States. *J. Appl. Meteor. Climatol.*, **47**, 475–497, https://doi.org/10.1175/2007JAMC1356.1.

Donat, M. G., L. V. Alexander, H. Yang, I. Durre, R. S. Vose, and J. Caesar, 2013: Global land-based datasets for monitoring climatic extremes. *Bull. Amer. Meteor. Soc.*, **94**, 997–1006, https://doi.org/10.1175/BAMS-D-12-00109.1.

Dunn, R. J. H., K. M. Willett, P. W. Thorne, E. Woolley, I. Durre, A. Dai, D. E. Parker, and R. S. Vose, 2012: HadISD: A quality controlled global synoptic report database for selected variables at long-term stations from 1973–2010. *Climate Past*, **8**, 1649–1679, https://doi.org/10.5194/cp-8-1649-2012.

Durre, I., M. J. Menne, B. E. Gleason, T. G. Houston, and R. S. Vose, 2010: Comprehensive automated quality assurance of daily surface observations. *J. Appl. Meteor. Climatol.*, **49**, 1615–1633, https://doi.org/10.1175/2010JAMC2375.1.

——, M. F. Squires, R. S. Vose, A. Arguez, W. S. Gross, J. R. Rennie, and C. J. Schreck, 2022: NOAA's nClimGrid-Daily version 1—Daily gridded temperature and precipitation for the contiguous United States since 1951. NOAA National Centers for Environmental Information, 6 May 2022, https://doi.org/10.25921/c4gt-r169.

Ensor, L. A., and S. M. Robeson, 2008: Statistical characteristics of daily precipitation: Comparisons of gridded and point datasets. *J. Appl. Meteor. Climatol.*, **47**, 2468–2476, https://doi.org/10.1175/2008JAMC1757.1.

Gervais, M., L. B. Tremblay, J. R. Gyakum, and E. Atallah, 2014: Representing extremes in a daily gridded precipitation

analysis over the United States: Impacts of station density, resolution, and gridding methods. *J. Climate*, **27**, 5201–5218, https://doi.org/10.1175/JCLI-D-13-00319.1.

Guttman, N. B., and C. B. Baker, 1996: Exploratory analysis of the difference between temperature observations recorded by ASOS and conventional methods. *Bull. Amer. Meteor. Soc.*, **77**, 2865–2874, https://doi.org/10.1175/1520-0477(1996)077<2865:EAOTDB>2.0.CO;2.

Haylock, M. R., N. Hofstra, A. M. G. Klein Tank, E. J. Klok, P. D. Jones, and M. New, 2008: A European daily high-resolution gridded data set of surface temperature and precipitation for 1950–2006. *J. Geophys. Res.*, **113**, D20119, https://doi.org/10.1029/2008JD010201.

Herrera, S., J. Fernández, and J. M. Gutiérrez, 2016: Update of the Spain02 gridded observational dataset for EURO-CORDEX evaluation: Assessing the effect of the interpolation methodology. *Int. J. Climatol.*, **36**, 900–908, https://doi.org/10.1002/joc.4391.

——, S. Kotlarski, P. M. Soares, R. M. Cardoso, A. Jaczewski, J. M. Gutiérrez, and D. Maraun, 2019: Uncertainty in gridded precipitation products: Influence of station density, interpolation method and grid resolution. *Int. J. Climatol.*, **39**, 3717–3729, https://doi.org/10.1002/joc.5878.

Hofstra, N., M. New, and C. McSweeney, 2009: The influence of interpolation and station network density on the distributions and trends of climate variables in gridded daily data. *Climate Dyn.*, **35**, 841–858, https://doi.org/10.1007/s00382-009-0698-1.

Huffman, G. J., R. F. Adler, M. M. Morrissey, S. Curtis, R. Joyce, B. McGavock, and J. Susskind, 2001: Global precipitation at one-degree daily resolution from multisatellite observations. *J. Hydrometeor.*, **2**, 36–50, https://doi.org/10.1175/1525-7541(2001)002<0036:GPAODD>2.0.CO;2.

Hutchinson, M. F., 1998a: Interpolation of rainfall data with thin plate smoothing splines: I. Two dimensional smoothing of data with short range correlation. *J. Geogr. Inf. Decis. Anal.*, **2**, 152–167.

——, 1998b: Interpolation of rainfall data with thin plate smoothing splines: II. Analysis of topographic dependence. *J. Geogr. Inf. Decis. Anal.*, **2**, 168–185.

——, 2007: ANUSPLIN version 4.37 user guide. Australian National University Centre for Resource and Environmental Studies Doc., 54 pp., https://vdocuments.mx/anusplin-version-437-user-guide.html.

——, D. W. McKenney, K. Lawrence, J. H. Pedlar, R. F. Hopkinson, E. Milewska, and P. Papadopol, 2009: Development and testing of Canada-wide interpolated spatial models of daily minimum–maximum temperature and precipitation for 1961–2003. *J. Appl. Meteor. Climatol.*, **48**, 725–741, https://doi.org/10.1175/2008JAMC1979.1.

Janis, M. J., 2002: Observation-time-dependent biases and departures for daily minimum and maximum air temperatures. *J. Appl. Meteor.*, **41**, 588–603, https://doi.org/10.1175/1520-0450(2002)041<0588:OTDBAD>2.0.CO;2.

Jarvis, C. H., and N. Stuart, 2001a: A comparison among strategies for interpolating maximum and minimum daily air temperatures. Part I: The selection of "guiding" topographic and land cover variables. *J. Appl. Meteor.*, **40**, 1060–1074, https://doi.org/10.1175/1520-0450(2001)040<1060:ACASFI>2.0.CO;2.

——, and ——, 2001b: A comparison among strategies for interpolating maximum and minimum daily air temperatures. Part II: The interaction between number of guiding variables and the type of interpolation method. *J. Appl. Meteor.*, **40**, 1075–1084, https://doi.org/10.1175/1520-0450(2001)040<1075:ACASFI>2.0.CO;2.

Karl, T. R., C. N. Williams Jr., W. M. Young, and P. M. Wendland, 1986: A model to estimate the time of observation bias associated with monthly mean maximum, minimum and mean temperatures for the United States. *J. Climate Appl. Meteor.*, **25**, 145–160, https://doi.org/10.1175/1520-0450(1986)025<0145:AMTETT>2.0.CO;2.

Livneh, B., T. J. Bohn, D. W. Pierce, F. Munoz-Arriola, B. Nijssen, R. Vose, D. R. Cayan, and L. Brekke, 2015: A spatially comprehensive, hydrometeorological data set for Mexico, the U.S., and southern Canada 1950–2013. *Sci. Data*, **2**, 150042, https://doi.org/10.1038/sdata.2015.42.

Menne, M. J., and C. N. Williams Jr., 2009: Homogenization of temperature series via pairwise comparisons. *J. Climate*, **22**, 1700–1717, https://doi.org/10.1175/2008JCLI2263.1.

——, and Coauthors, 2012a: Global Historical Climatology Network–Daily (GHCN-Daily), version 3. NOAA National Centers for Environmental Information, 1 April 2017, https://doi.org/10.7289/V5D21VHZ.

——, I. Durre, R. S. Vose, B. E. Gleason, and T. G. Houston, 2012b: An overview of the Global Historical Climatology Network–Daily database. *J. Atmos. Oceanic Technol.*, **29**, 897–910, https://doi.org/10.1175/JTECH-D-11-00103.1.

Myrick, D. T., and J. D. Horel, 2008: Sensitivity of surface analyses over the western United States to RAWS observations. *Wea. Forecasting*, **23**, 145–158, https://doi.org/10.1175/2007WAF2006074.1.

Newman, A. J., and Coauthors, 2015: Gridded ensemble precipitation and temperature estimates for the contiguous United States. *J. Hydrol.*, **16**, 2481–2500, https://doi.org/10.1175/JHM-D-15-0026.1.

Palmer, W. C., 1965: Meteorological drought. U.S. Weather Bureau Research Paper 45, 58 pp.

Serreze, M. C., M. P. Clark, and R. L. Armstrong, 1999: Characteristics of the western United States snowpack from snowpack telemetry (SNOTEL) data. *Water Resour. Res.*, **35**, 2145–2160, https://doi.org/10.1029/1999WR900090.

Thorne, P. W., and Coauthors, 2016: Reassessing changes in diurnal temperature range: Intercomparison and evaluation of existing global dataset estimates. *J. Geophys. Res. Atmos.*, **121**, 5138–5158, https://doi.org/10.1002/2015JD024584.

Thornton, P. E., S. W. Running, and M. A. White, 1997: Generating surfaces of daily meteorological variables over large regions of complex terrain. *J. Hydrol.*, **190**, 214–251, https://doi.org/10.1016/S0022-1694(96)03128-9.

——, R. Shrestha, M. Thornton, S. Kao, Y. Wei, and B. E. Wilson, 2021: Gridded daily weather data for North America with comprehensive uncertainty quantification. *Sci. Data*, **8**, 190, https://doi.org/10.1038/s41597-021-00973-0.

Vose, R. S., and Coauthors, 2014: Improved historical temperature and precipitation time series for U.S. climate divisions. *J. Appl. Meteor. Climatol.*, **53**, 1232–1251, https://doi.org/10.1175/JAMC-D-13-0248.1.

Wagner, P. D., P. Fiener, F. Wilken, S. Kumar, and K. Schneider, 2012: Comparison and evaluation of spatial interpolation schemes for daily rainfall in data scarce regions. *J. Hydrol.*, **464–465**, 388–400, https://doi.org/10.1016/j.jhydrol.2012.07.026.

Walton, D., and A. Hall, 2018: An assessment of high-resolution gridded temperature datasets over California. *J. Climate*, **31**, 3789–3810, https://doi.org/10.1175/JCLI-D-17-0410.1.

Willmott, C. J., C. M. Rowe, and W. D. Philpot, 1985: Small-scale climate maps: A sensitivity analysis of some common assumptions associated with grid-point interpolation and contouring. *Amer. Cartographer*, **12**, 5–16, https://doi.org/10.1559/152304085783914686.

Zachariassen, J., K. F. Zeller, N. Nikolov, and T. McClelland, 2003: A review of the Forest Service Remote Automated Weather Station (RAWS) network. U.S. Forest Service Rocky Mountain Research Station Tech. Rep. RMRSGTR-119, 153 pp., http://www.fs.fed.us/rm/pubs/rmrs_gtr119.pdf.